A Computerized Microelectrode Recording to Magnetic Resonance Imaging Mapping System for Subthalamic Nucleus Deep Brain Stimulation Surgery

Sunjay S. Dodani, PhD[*‡§]
Charles W. Lu, MS[*‡§]
J. Wayne Aldridge, PhD[*‡¶]
Kelvin L. Chou, MD[*‡§]
Parag G. Patil, MD, PhD[*‡§‖]

[*]Surgical Therapies Improving Movement Program, University of Michigan, Ann Arbor, Michigan; [‡]Department of Neurosurgery, University of Michigan, Ann Arbor, Michigan; [§]Department of Neurology, University of Michigan, Ann Arbor, Michigan; [¶]Department of Psychology, University of Michigan, Ann Arbor, Michigan; [‖]Department of Biomedical Engineering, University of Michigan, Ann Arbor, Michigan

A preliminary version of this work was submitted to the Biennial Meeting of the American Society for Stereotactic and Functional Neurosurgery in Washington, DC, May 31-June 3, 2014, as a poster presentation.

Correspondence:
Parag G. Patil, MD, PhD,
Surgical Therapies Improving Movement Program,
University of Michigan Health System,
1500 East Medical Center Drive,
SPC 5338,
Ann Arbor, MI 48109-5338.
E-mail: pgpatil@umich.edu

Received, September 30, 2016.
Accepted, July 11, 2017.
Published Online, August 5, 2017.

BACKGROUND: Accurate electrode placement is critical to the success of deep brain stimulation (DBS) surgery. Suboptimal targeting may arise from poor initial target localization, frame-based targeting error, or intraoperative brain shift. These uncertainties can make DBS surgery challenging.

OBJECTIVE: To develop a computerized system to guide subthalamic nucleus (STN) DBS electrode localization and to estimate the trajectory of intraoperative microelectrode recording (MER) on magnetic resonance (MR) images algorithmically during DBS surgery.

METHODS: Our method is based upon the relationship between the high-frequency band (HFB; 500-2000 Hz) signal from MER and voxel intensity on MR images. The HFB profile along an MER trajectory recorded during surgery is compared to voxel intensity profiles along many potential trajectories in the region of the surgically *planned* trajectory. From these comparisons of HFB recordings and potential trajectories, an estimate of the MER trajectory is calculated. This *calculated* trajectory is then compared to *actual* trajectory, as estimated by postoperative high-resolution computed tomography.

RESULTS: We compared 20 *planned*, *calculated*, and *actual* trajectories in 13 patients who underwent STN DBS surgery. Targeting errors for our *calculated* trajectories (2.33 mm $\pm$ 0.2 mm) were significantly less than errors for surgically *planned* trajectories (2.83 mm $\pm$ 0.2 mm; $P = .01$), improving targeting prediction in 70% of individual cases (14/20). Moreover, in 4 of 4 initial MER trajectories that missed the STN, our method correctly indicated the required direction of targeting adjustment for the DBS lead to intersect the STN.

CONCLUSION: A computer-based algorithm simultaneously utilizing MER and MR information potentially eases electrode localization during STN DBS surgery.

KEY WORDS: Deep brain stimulation, Electrophysiology, Magnetic resonance imaging, Microelectrode recording, Parkinson disease, Subthalamic nucleus

Operative Neurosurgery 14:661–667, 2018 DOI: 10.1093/ons/opx169

Deep brain stimulation (DBS) is a well-established surgical therapy for Parkinson's disease.[1] Bilateral chronic high-frequency stimulation of the subthalamic nucleus (STN) alleviates the motor symptoms of Parkinson's disease.[2-8] Targeting of the STN has been traditionally performed indirectly using data from standardized stereotactic atlases.[9,10] In recent years, direct visualization of the STN with magnetic resonance imaging (MRI) has become possible using a range of magnetic field strengths (1.5 T-9.4 T). This advancement in imaging has eased preoperative targeting of the STN in DBS surgery.[11]

However, with the loss of cerebrospinal fluid and the buildup of intracranial air during DBS surgery,[12] the brain may shift from what is visualized on preoperative MRI, creating a misalignment with the planned target for DBS (brain shift).[13,14] In addition, there are intrinsic inaccuracies in frame-based targeting (frame

ABBREVIATIONS: CT, computed tomography; **DBS,** deep brain stimulation; **HFB,** high-frequency band; **MER,** microelectrode recording; **MR,** magnetic resonance; **MRI,** magnetic resonance imaging; **STN,** subthalamic nucleus

inaccuracy).[15] To accommodate these errors and shifts, microelectrode recording (MER) may be used intraoperatively to confirm the location of the STN.[16-20] Intraoperative signal analysis from MER has been shown to have good correlation with visualized subcortical structural borders, including the STN, from magnetic resonance (MR) images.[11,21,22] In addition, the analysis of high-frequency band (HFB) signals from MER has provided quantitative information regarding the identity of physiological structures during DBS surgery.[23,24]

Even with these advances in MER and MRI resolution, surgeons lack the tools to precisely and objectively localize an intraoperative MER trajectory in frame-based stereotactic coordinates. The average error between the *planned* surgical targeting and the *actual* postoperative DBS lead location for frame-based targeting has been historically 2 to 3 mm, although more recent targeting methods have achieved accuracy of <1.5 mm.[15] The STN itself may be reliably differentiated from the zona incerta and substantia nigra with traditional MER. However, while the presence of motor-responsive cells allows some differentiation of motor areas from limbic/associative areas within the STN, precise localization within the STN region is difficult, since MER characteristics throughout the STN are broadly similar. More accurate localization of MER trajectories during surgery could allow for improved accuracy of DBS lead placement in the STN region. Furthermore, an automated, computer-based algorithm to perform MER trajectory localization could potentially increase operative speed and decrease reliance on the subjective judgment and availability of specialized electrophysiologists.

In this study, we utilize a novel computer-based algorithm to automatically map intraoperative MER recordings to individual MR images for STN DBS patients. We find that HFB signals in MER recordings closely relate to 3-T MR voxel intensity in the STN region, a novel finding. To evaluate the merits of this approach, we compared surgically *planned* trajectories and our algorithmically *calculated* MER trajectories to postoperative *actual* lead locations (Figure 1). We find that *calculated* trajectories are closer to *actual* lead locations than the *planned* trajectories, indicating the potential for our automated algorithm to improve the accuracy of lead placement in STN DBS surgery.

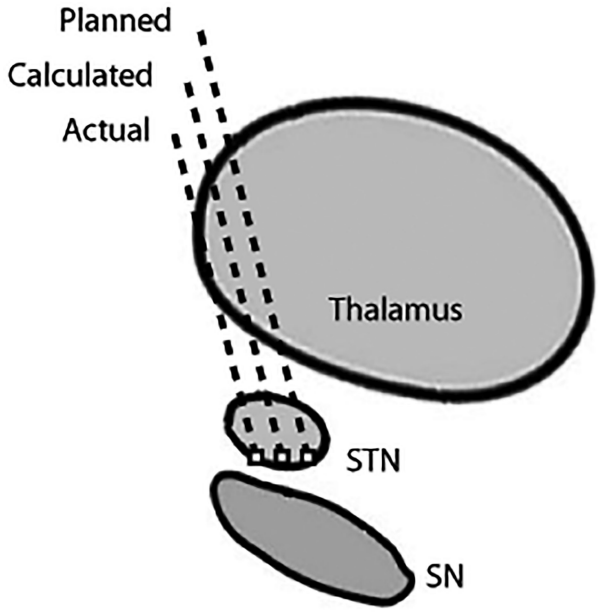

FIGURE 1. *Illustration defining trajectory terminology. "Planned" indicates the location of the surgically planned trajectory. "Actual" indicates the actual location of the DBS lead trajectory on postoperative computed tomography (CT). "Calculated" indicates the location of the intraoperative microelectrode trajectory, as calculated by the automated algorithm. The thalamus, STN, and substantia nigra structures are indicated. In this illustration, the calculated trajectory lies closer to the actual lead location than the surgical plan, indicating that the algorithm has improved lead localization estimation. SN, substantia nigra.*

METHODS

Patient Selection

We studied 13 consecutive patients with advanced idiopathic Parkinson's disease who underwent STN DBS surgery at our institution (9 men, 4 women; age, 66 ± 6 yr; range, 52-73 yr). Patient-selection criteria for DBS have been described previously in detail.[11,14,25] STN DBS patients had an established diagnosis of Parkinson's disease and had motor fluctuations not well controlled by medications or had levodopa-unresponsive tremor. Patients with contraindications to 3-T MRI scanning or structural abnormalities in the brain were excluded from this study. We performed the study in accordance with the policies of the Medical Institutional Review Board of the University of Michigan. All subjects gave written informed consent.

DBS Surgery

The details of our DBS surgical procedure are also described in a previous publication.[11] Patients underwent preoperative 3-T MRI using a validated protocol to visualize the STN (Table 1).[11] On the day of surgery, patients were fitted with a Leksell stereotactic frame (Elekta Instruments AB, Stockholm, Sweden), and underwent a preoperative 1.5 T MR scan that was coregistered to the preoperative 3-T MRI (Analyze 9.0; AnalyzeDirect, Inc, Overland Park, Kansas). Frame-based surgical planning was then performed using commercial software (Framelink; Medtronic, Inc, Dublin, Ireland). MER was performed prior to the insertion of each DBS lead. MER signals were recorded using a bipolar microelectrode (MicroTargeting Electrode; FHC, Bowdin, Maine), amplified (D360 Isolated Patient Amplifier System; Digitimer Inc, Hertfordshire, England), and recorded to a computer using custom software (LabView; National Instruments, Austin, Texas). The planned targets were initially assigned from indirect targeting (12 mm lateral, 3 mm posterior, and 4 mm inferior to the mid-commissural point) with adjustment from direct 3-T STN visualization to the ventral border of STN. Recordings were performed from 15 mm above to 5 mm below the planned target. The microelectrode was advanced in 0.1 mm to 0.5 mm steps, and held in position at each depth for 8 s to record extracellular signals. An electrophysiologist identified the dorsal and ventral borders of the STN during surgery. DBS leads were then inserted with the tip

TABLE 1. MRI Protocol

Philips Achieva 3-T MRI scanner settings	
Slice orientation	COR
Field of view	FH 200
Voxel size	FH 0.69
	RL 0.69
	AP 1.25
Slice thickness	1.25
Gap	0
SENSE factor	1.8
#Slices	40
Foldover direction	R/L
Scan mode	3D
Technique	IR
Fast imaging mode	TSE
TSE factor	58
TE	200
TR	6000
NSA	1
Scan duration	7:18

Abbreviations: TSE = turbo spin echo, TE = echo time, TR = repetition time, NSA = number of signal averages.
From Patil PG, Conrad EC, Aldridge JW, Chenevert TL, Chou KL. The anatomical and electrophysiological subthalamic nucleus visualized by 3-T magnetic resonance imaging. *Neurosurgery.* 2012;71(6):1089-1095; discussion 1095. By permission of the Congress of Neurological Surgeons.

TABLE 2. CT Imaging Protocol

GE HD750 64-slice CT scanner	
Scan type	Axial
HiRes mode	On
Gantry rotation time/length	1.0 s full
Detector coverage	20 mm
Slice thickness	0.625 mm
# of images/rotation	32i
Interval	20 mm
KVP/mA	140/450
ASIR %	SS40
Recon mode	Full
DFOV	27-29 cm
SFOV	Head
Algorithm	HD standard

Abbreviations: DFOV = display field of view, ASIR = adaptive statistical iterative reconstruction, KVP = peak kilovoltage, SFOV = scan field of view.
From Patil PG, Conrad EC, Aldridge JW, Chenevert TL, Chou KL. The anatomical and electrophysiological subthalamic nucleus visualized by 3-T magnetic resonance imaging. *Neurosurgery.* 2012;71(6):1089-1095; discussion 1095. By permission of the Congress of Neurological Surgeons.

near the ventral border of the electrophysiologically identified STN. A high-resolution computed tomographic scan was performed 2 to 4 wk after surgery to visualize the location of the DBS leads and individual contacts (Table 2).

Generation and Scoring of Voxel-Based Potential Trajectories

DBS trajectories at different locations correspond to different profiles of voxel intensity on MRI, corresponding to the deep brain nuclei that they traverse (Figure 2A). Candidate trajectory vectors were generated from MRI and scored against HFB power (Figure 2B). Candidate vectors had starting points within an 8 × 8 × 8 voxel cube, centered at the start coordinate of MER recording, and passed within an 8 × 8 × 8 voxel cube centered at the planned target coordinate. Candidate vectors were restricted to trajectories of the same length as the MER recording, and within 3° of the surgical plan. For the typical MER recording with a 20-mm trajectory, over 10 000 potential trajectories were scored. Note that some trajectories, while uniquely defined in the algorithm, partially superimpose in practice due to finite voxel resolution and trajectory superposition.

Each candidate trajectory was scored against HFB power for the associated single-channel MER recordings (Figure 2C). Unit normalized (0-1) HFB spectral power (500-2000 Hz) at each recorded depth was calculated after the removal of large action-potential spikes using a custom software algorithm (MATLAB, MathWorks, Inc, Natick, Massachusetts). Unit normalized (0-1) voxel intensities along each potential trajectory were then calculated. Voxel intensity was inverted prior to normalization so that greater voxel score corresponds to darker, gray-matter structures on MRI. To compare HFB power to voxel intensity, the average absolute difference between normalized HFB power and normalized voxel intensity was determined for each potential trajectory. Once all potential trajectories were scored, the top 7% of potential trajectories were spatially averaged to produce the calculated trajectory estimate (Figure 3). A 7% threshold was empirically selected by regression analysis as the threshold that best minimized the distance between the calculated trajectory and the actual electrode position.

Statistical Analysis

Statistical analysis was performed with commercially available software (MATLAB, MathWorks, Inc; Excel, Microsoft Inc, Redmond, Washington). Paired 2-tailed *t*-tests were used to calculate *P*-values for trajectory data comparing calculated trajectory distances to planned trajectory distances. Distances between the actual DBS electrode trajectory, the planned trajectory, and the calculated trajectory estimate were measured at the Z coordinate of the planned target. Distances in millimeters represent the 2-dimensional distance of the X and Y coordinates at the planned Z coordinate for every trajectory. Results are reported as mean ± Standard Error of the Mean unless otherwise noted.

RESULTS

A total of 20 MER trajectory datasets from 13 consecutive STN DBS patients were available for analysis. For 14 of 20 MER trajectories, adequate STN activity was observed along the MER trajectory, the DBS electrode was immediately inserted along the same trajectory, and intraoperative DBS stimulation revealed good symptom control without undesirable side effects. These 14 trajectories were utilized to compare *planned* trajectory, *calculated* trajectory, and *actual* lead trajectory (Figure 1). In 4 of 20 remaining MER trajectories, insufficient STN activity was observed. In these 4 cases, targeting was redirected and MER recording was performed along a new trajectory. Finally, in the

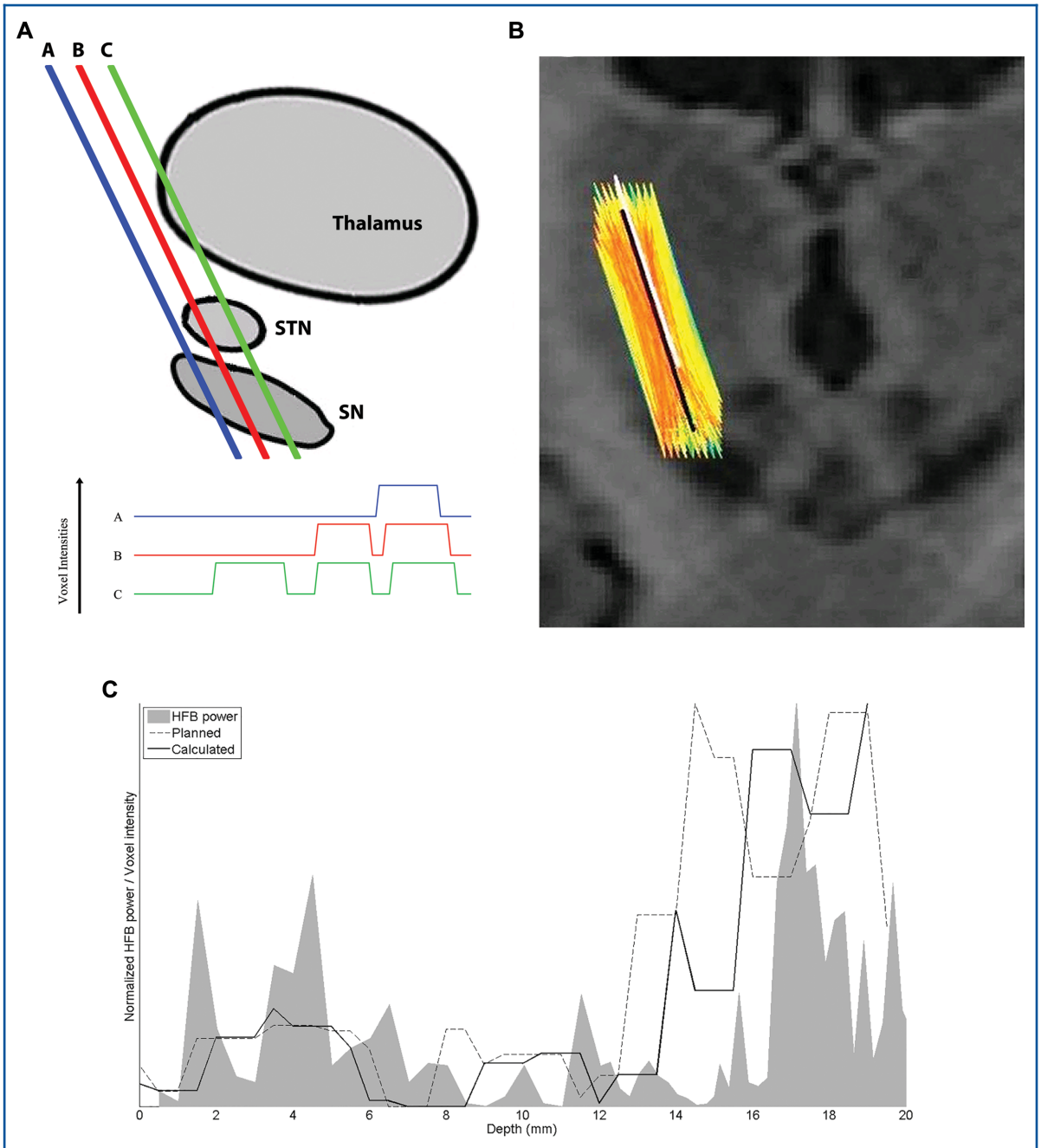

FIGURE 2. *The automated algorithm.* **A**, *MR voxel intensity profile schema. Illustrative color-coded trajectories through thalamus, subthalamic nucleus, and substantia nigra are shown on an MR imaging schema (above) with corresponding color-coded voxel intensities (below). Note inversion such that positive deviations in the voxel intensity profile (below) correspond to regions of gray matter along the color-corresponding exemplar trajectory (above).* **B**, *Trajectories superimposed on 3-T coronal MR image of a patient. The surgically planned trajectory is shown in white; potential candidate trajectories used to determine the calculated trajectory are colored according to score (red: higher score, yellow: intermediate score, green: lower score). Note declining scores with distance from the planned trajectory. The final calculated trajectory is shown in black.* **C**, *Relationship of high-frequency band power to voxel intensity. HFB power (gray solid) superimposed with voxel intensity profile along the surgical plan (dashed line) and algorithm-calculated estimate (solid line) for a single trajectory. The target depth, at 15 mm, corresponds to the ventral border of STN. Noise within the data necessitates averaging of multiple, higher scoring potential trajectories to estimate the final calculated trajectory. SN, substantia nigra.*

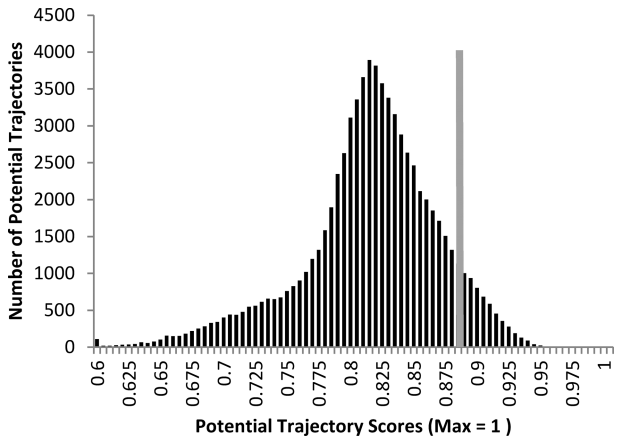

FIGURE 3. *Determination of the calculated trajectory estimate from scored potential trajectories. The plot indicates the score distribution of 40 000 potential trajectories in the region of a single surgical plan. The top 7% of potential trajectories (scores ≥ 0.886), marked with a gray vertical line, are spatially averaged to estimate the final calculated trajectory. Due to superposition, voxel size, directional constraints, and path length constraints, some potential trajectories may superimpose.*

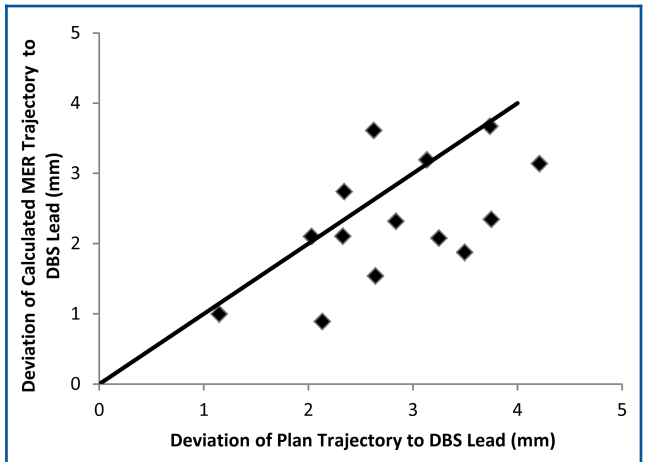

FIGURE 4. *Comparison of algorithm-estimated and surgically planned trajectories. Distances between surgically planned and actual trajectories (X-axis) are plotted against distances between calculated and actual trajectories (Y-axis). Points below the solid line represent cases in which the accuracy of the algorithm exceeds that of the surgical plan, while points above the line represent the opposite.*

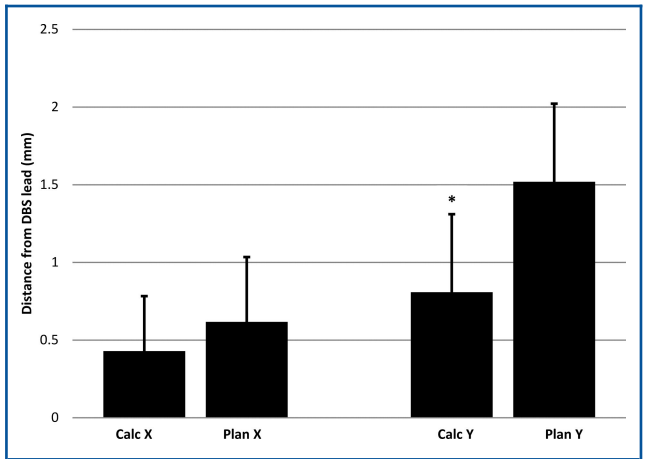

FIGURE 5. *Comparison of algorithm-estimated and surgically planned trajectories in the axial plane of the target z-coordinate. Distances to the actual DBS lead trajectory are shown for calculated trajectories (Calc) and the surgically planned trajectories (Plan), in the mediolateral (X), and anteroposterior (Y) dimensions. Note the proportionate improvements in accuracy that are apparent for both X- and Y-coordinates, although only Y-axis improvements were statistically significant.*

remaining 2 of 20 trajectories, intraoperative DBS stimulation was associated with undesirable side effects or poor symptom control. In these 2 cases, the DBS lead was repositioned to a new trajectory without additional MER recording, precluding further analysis.

We first evaluated the overall expected improvement in localization accuracy through use of the automated algorithm (Figures 2, 3, and Methods). We compared the average distance from 14 *planned* and *calculated* trajectories to the *actual* trajectory of the DBS lead. The average distance from the calculated trajectory estimate to the actual lead trajectory was 2.33 ± 0.2 mm. The distance from the surgically planned trajectory to the actual lead trajectory was 2.83 ± 0.2 mm. The 0.5 mm average improvement in lead localization was statistically significant ($P = .01$).

Since not only average localization improvement, but also individual localization improvement is of critical importance, we examined the impact of our algorithm at the individual case level (Figure 4). There is significant correlation between the distance of the calculated trajectory to the actual lead trajectory and the distance of the planned trajectory to the actual lead trajectory ($r = 0.58$, $P = .02$). Importantly, of the 14 MER trajectories analyzed, 10 of 14 calculated trajectories were closer to the actual DBS lead position than the surgically planned trajectory and an additional 2 of 14 trajectories showed no difference, suggesting that in 12 of 14 cases, the performance of the automated algorithm allowed as good or better estimation of lead position than the initial surgical plan.

To evaluate our algorithm in greater detail, we examined deviations along frame-coordinate dimensions (Figure 5). Deviations from the surgically planned trajectory to actual trajectory in the axial plane of the target may deviate along the mediolateral (X) or the anteroposterior (Y) dimensions. For our automated algorithm, the average Y-coordinate distance of the calculated to actual trajectories (0.80 ± 0.50 mm) was significantly closer than planned to actual trajectories (1.52 ± 0.50 mm, $P < .001$). The X-coordinate distance for the calculated trajectories (0.43 ± 0.35 mm) was not statistically closer to the actual trajectories than

the planned trajectories (0.62 ± 0.42 mm, $P = .19$). Note that X-coordinate errors were significantly smaller than Y-coordinate errors.

We also evaluated the 4 first pass MER trajectories with our scoring method to determine if the direction and magnitude of adjustment of the subsequent final trajectory could be predicted. The average adjustment made by the neurosurgeon after each of these tracks was 2 mm anterior to the first pass, the minimum allowed by the microdrive system. The automated algorithm calculated the correct directional shift but with a smaller magnitude than that performed by the neurosurgeon: 0.46 ± 0.1 mm in the anterior direction.

DISCUSSION

The effectiveness of STN DBS surgery for Parkinson's disease is dependent upon the accuracy of lead placement. Targeting the STN traditionally involves using an imaging method to define an initial stereotactic target and then using intraoperative MER and clinical testing to optimally position the DBS electrode. Advancements in imaging technology now enable direct visualization of the STN and have improved targeting accuracy.[11,15,22] However, targeting errors remain due to frame inaccuracy and brain shifts during surgery.[14,15] To accommodate targeting error and variability in the stereotactic location of the target structure, MER recordings help neurosurgeons and electrophysiologists to compensate for targeting errors.[23,24,26]

In this study, we used 3-T MRI voxel intensities and quantitative analysis of the HFB signal to quantitatively and algorithmically estimate the location of the MER trajectory during STN DBS surgery. Our results demonstrate that the *calculated* MER trajectory, produced by the computer-based algorithm, is significantly closer to *actual* postoperative DBS lead location than the surgically *planned* trajectory. Furthermore, since the calculation was performed rapidly, automatically, quantitatively, and algorithmically, the approach potentially minimizes the need for time-intensive, subjective human electrophysiological interpretation. We anticipate that the algorithm could be used after MER recording along a single-channel trajectory to map the location of the MER trajectory to MRI.

In this study, 1 limitation to our measure of accuracy is the surgical uncertainty of final lead placement. The distance between the *calculated* and *actual* trajectories may primarily result from deviations of the DBS lead trajectory from true after insertion through the guiding cannula. Although the cannula provides a rigid path for the DBS lead to travel toward the target, there are typically slight, unknown deviations between the end of the cannula and target depth. These deviations appear as trajectory error in our study.

A basic scoring method was used to evaluate potential voxel trajectories compared to the HFB power signal recorded from MER. This method was validated through simulation (not shown) to ensure accurate scores and locations were assigned to each potential voxel trajectory. We found this method to be robust and efficient when tested with known trajectory locations. In every test of fixed and variable trajectory locations, the scoring method correctly identified the actual trajectory. For our study, we chose a large enough search window to account for the observed error between the planned target and the DBS lead (2.83 ± 0.2 mm). We confined our search space for potential trajectories to approximately 4 mm. This may have limited our study from verifying our results with larger search windows. Additionally, our observed targeting error (2.83 ± 0.2 mm) is similar to previous studies in frame-based systems, but greater than some recent studies.[15] Hence, though the algorithm provides targeting benefits, greater algorithmic accuracy may be required to maintain this advantage with newer, more accurate DBS targeting methods. Finally, we observed significantly greater targeting error in the Y-dimension than the X-dimension (Figure 5). Greater Y errors are a common feature of frame-based studies of DBS targeting,[15] and may potentially be influenced by frame geometry, brain-shift, gravity, or the greater angle of incidence in Y versus X directions.

Of the MER trajectories available for analysis in our study, 4 were categorized as "first tracks." These were trajectories that did not provide sufficient electrophysiological confirmation of the STN and thus required a subsequent MER track in an alternative location. The automated method provided the information necessary to determine the direction to shift the subsequent MER trajectory, ie a shift anterior, posterior, medial, or lateral of the planned target. However, due to the limited resolution (2 mm shifts) and direction of adjustment in our surgical setup, we were unable to draw any significant conclusions regarding the magnitude of shift necessary to reach the intended target.

This method could potentially be used to automate and to visualize the MER process while possibly reducing surgical time, risk, and error. Following MER recording along a trajectory, the algorithm requires only a few minutes to run during DBS surgery. Its application may enable neurosurgeons that are less familiar with DBS surgery to do the procedure more readily. Algorithmic analysis of MER and MRI targeting may eventually allow reduced dependence upon specialized electrophysiology training. However, although our study data suggest that calculating the position of a microelectrode with HFB and image analysis may be performed automatically, without the need to analyze either subjectively, this method cannot completely replace intraoperative electrophysiological monitoring given that intraoperative clinical testing is necessary to confirm that the electrode location is optimally effective.

CONCLUSION

With advancements in MRI technology and the quantitative analysis of HFB electrophysiology signals, we present a novel method for locating and visualizing microelectrode trajectories intraoperatively. We used 3-T MRI voxel intensities and

quantitative analysis of the HFB signal from MER to better estimate the locations of microelectrode trajectories for patients with Parkinson disease undergoing STN DBS. These results demonstrated that the calculated position of the MER trajectory was significantly closer to the DBS lead than the surgically planned trajectory was to the DBS lead. This novel method may improve DBS surgery by reducing surgical error and duration compared to current methods of DBS targeting.

Disclosures

This research was funded by the A. Alfred Taubman Medical Institute, the Coulter Foundation, and the STIM (Surgical Therapies Improving Movement) Program. The authors have no personal, financial, or institutional interest in any of the drugs, materials, or devices described in this article.

REFERENCES

1. Benabid AL, Chabardes S, Mitrofanis J, Pollak P. Deep brain stimulation of the subthalamic nucleus for the treatment of Parkinson's disease. *Lancet Neurol*. 2009;8(1):67-81.
2. Krack P, Benazzouz A, Pollak P, et al. Treatment of tremor in Parkinson's disease by subthalamic nucleus stimulation. *Mov Disord*. 1998;13(6):907-914.
3. Benabid AL, Pollak P, Gross C, et al. Acute and long-term effects of subthalamic nucleus stimulation in Parkinson's disease. *Stereotact Funct Neurosurg*. 1994;62(1-4):76-84.
4. Krack P, Pollak P, Limousin P, Benazzouz A, Benabid AL. Stimulation of subthalamic nucleus alleviates tremor in Parkinson's disease. *Lancet*. 1997;350(9092):1675.
5. Kumar R, Lozano AM, Kim YJ, et al. Double-blind evaluation of subthalamic nucleus deep brain stimulation in advanced Parkinson's disease. *Neurology*. 1998;51(3):850-855.
6. Lang AE. Surgery for Parkinson disease: a critical evaluation of the state of the art. *Arch Neurol*. 2000;57(8):1118-1125.
7. Rodriguez-Oroz MC, Zamarbide I, Guridi J, Palmero MR, Obeso JA. Efficacy of deep brain stimulation of the subthalamic nucleus in Parkinson's disease 4 years after surgery: double blind and open label evaluation. *J Neurol Neurosurg Psychiatry*. 2004;75(10):1382-1385.
8. Liang GS, Chou KL, Baltuch GH, et al. Long-term outcomes of bilateral subthalamic nucleus stimulation in patients with advanced Parkinson's disease. *Stereotact Funct Neurosurg*. 2006;84(5-6):221-227.
9. Trottenberg T, Kupsch A, Schneider GH, Brown P, Kuhn AA. Frequency-dependent distribution of local field potential activity within the subthalamic nucleus in Parkinson's disease. *Exp Neurol*. 2007;205(1):287-291.
10. Schaltenbrand G, Wahren W, Hassler R. *Atlas for Stereotaxy of the Human Brain*. 2nd ed. Chicago: Stuttgart Thieme; 1977.
11. Patil PG, Conrad EC, Aldridge JW, Chenevert TL, Chou KL. The anatomical and electrophysiological subthalamic nucleus visualized by 3-T magnetic resonance imaging. *Neurosurgery*. 2012;71(6):1089-1095; discussion 1095.
12. Hunsche S, Sauner D, Maarouf M, et al. Intraoperative X-ray detection and MRI-based quantification of brain shift effects subsequent to implantation of the first electrode in bilateral implantation of deep brain stimulation electrodes. *Stereotact Funct Neurosurg*. 2009;87(5):322-329.
13. Umemura A, Oka Y, Yamada K, Oyama G, Shimo Y, Hattori N. Validity of single tract microelectrode recording in subthalamic nucleus stimulation. *Neurol Med Chir (Tokyo)*. 2013;53(11):821-827.
14. Bentley JN, Guan Z, Cummings KS, Chou KL, Patil PG. Influence of intracranial air on electrode position and clinical outcomes following deep brain stimulation for Parkinson's disease. *Stereotact Funct Neurosurg*. 2017;95(1):6-12.
15. Li Z, Zhang JG, Ye Y, Li X. Review on factors affecting targeting accuracy of deep brain stimulation electrode implantation between 2001 and 2015. *Stereotact Funct Neurosurg*. 2016;94(6):351-362.
16. Holloway KL, Gaede SE, Starr PA, Rosenow JM, Ramakrishnan V, Henderson JM. Frameless stereotaxy using bone fiducial markers for deep brain stimulation. *J Neurosurg*. 2005;103(3):404-413.
17. Starr PA, Christine CW, Theodosopoulos PV, et al. Implantation of deep brain stimulators into the subthalamic nucleus: technical approach and magnetic resonance imaging-verified lead locations. *J Neurosurg*. 2002;97(2):370-387.
18. Bejjani BP, Dormont D, Pidoux B, et al. Bilateral subthalamic stimulation for Parkinson's disease by using three-dimensional stereotactic magnetic resonance imaging and electrophysiological guidance. *J Neurosurg*. 2000;92(4):615-625.
19. Sterio D, Zonenshayn M, Mogilner AY, et al. Neurophysiological refinement of subthalamic nucleus targeting. *Neurosurgery*. 2002;50(1):58-67.
20. Hutchison WD, Allan RJ, Opitz H, et al. Neurophysiological identification of the subthalamic nucleus in surgery for Parkinson's disease. *Ann Neurol*. 1998;44(4):622-628.
21. Hamani C, Richter EO, Andrade-Souza Y, Hutchison W, Saint-Cyr JA, Lozano AM. Correspondence of microelectrode mapping with magnetic resonance imaging for subthalamic nucleus procedures. *Surg Neurol*. 2005;63(3):249-253; discussion 253.
22. Coste J, Ouchchane L, Sarry L, et al. New electrophysiological mapping combined with MRI in parkinsonian's subthalamic region. *Eur J Neurosci*. 2009;29(8):1627-1633.
23. Novak P, Daniluk S, Ellias SA, Nazzaro JM. Detection of the subthalamic nucleus in microelectrographic recordings in Parkinson disease using the high-frequency (>500 hz) neuronal background. Technical note. *J Neurosurg*. 2007;106(1):175-179.
24. Novak P, Przybyszewski AW, Barborica A, Ravin P, Margolin L, Pilitsis JG. Localization of the subthalamic nucleus in Parkinson disease using multiunit activity. *J Neurol Sci*. 2011;310(1-2):44-49.
25. Houshmand L, Cummings KS, Chou KL, Patil PG. Evaluating indirect subthalamic nucleus targeting with validated 3-tesla magnetic resonance imaging. *Stereotact Funct Neurosurg*. 2014;92(6):337-345.
26. Gross RE, Krack P, Rodriguez-Oroz MC, Rezai AR, Benabid AL. Electrophysiological mapping for the implantation of deep brain stimulators for Parkinson's disease and tremor. *Mov Disord*. 2006;21(suppl 14):S259-S283.

Acknowledgments

The authors wish to thank Karen S. Cummings, Susan V. Grube, and the members of the STIM program for their clinical and technical assistance.

COMMENT

The authors present results from a preliminary study utilizing a novel algorithm which combines MRI and electrophysiological (MER) data to predict the actual location of a DBS electrode, and its deviation from the planned location in stereotactic space. Their results suggest that the "true" trajectory generated by their algorithm is closer to the actual final lead location than their planned trajectory.

The authors' findings are not unexpected. With advances in imaging allowing direct visualization of target nuclei, errors in targeting are most likely due to a combination of the inherent error in the stereotactic frame or other delivery system, as well as brain shift. Simply put, we know where we want to put the lead, but we don't always put it where we think we're putting it. The growing body of literature demonstrating that asleep image-guided DBS produces clinical outcomes on par with awake physiologic-based implantation suggests that the alternative explanation, namely that the target is not optimal due to physiologic variations between individuals, is now less likely.

This method may be beneficial as a surrogate for intraoperative imaging in those centers where intraoperative imaging is not available, or when contraindicated.

Alon Y. Mogilner
New York, New York